Ultramicroscopy 109 (2009) 1211–1216

Contents lists available at ScienceDirect

Ultramicroscopy

journal homepage: www.elsevier.com/locate/ultramic

# Quantitative measurements of Kikuchi bands in diffraction patterns of backscattered electrons using an electrostatic analyzer

M.R. Went [a], A. Winkelmann [b], M. Vos [a,*]

[a] Atomic and Molecular Physics Laboratories, Research School of Physics and Engineering, Australian National University, Canberra ACT 0200, Australia
[b] Max-Planck-Institut für Mikrostrukturphysik, Weinberg 2, D-06120 Halle (Saale), Germany

ARTICLE INFO

*Article history:*
Received 27 January 2009
Received in revised form
24 April 2009
Accepted 5 May 2009

*PACS:*
61.85.+p
61.05.jd

*Keywords:*
Electron backscatter diffraction
Kikuchi pattern
Electrostatic analyzer

ABSTRACT

Diffraction patterns of backscattered electrons can provide important crystallographic information with high spatial resolution. Recently, the dynamical theory of electron diffraction was applied to reproduce in great detail backscattering patterns observed in the scanning electron microscope (SEM). However, a fully quantitative comparison of theory and experiment requires angle-resolved measurements of the intensity and the energy of the backscattered electrons, which is difficult to realize in an SEM. This paper determines diffraction patterns of backscattered electrons using an electrostatic analyzer, operating at energies up to 40 keV with sub-eV energy resolution. Measurements are done for different measurement geometries and incoming energies. Generally a good agreement is found between theory and experiment. This spectrometer also allows us to test the influence of the energy loss of the detected electron on the backscattered electron diffraction pattern. It is found that the amplitude of the intensity variation decreases only slowly with increasing energy loss from 0 to 60 eV.



## 1. Introduction

Electrons that are backscattered from crystalline samples can show intricate intensity distributions. Diffraction spots are formed by coherent scattering of the incident beam by the crystal, while patterns called Kikuchi patterns [1,2] are produced after backscattering from individual incoherent sources.

In a scanning electron microscope (SEM), the Kikuchi patterns of backscattered electrons with 5–40 keV kinetic energy can be observed in a straightforward way on a phosphor screen placed near the sample and imaged by a sensitive CCD camera. This specific technique is called "electron backscatter diffraction" (EBSD) [3]. It is routinely used to determine the crystal phase and orientation of grains in polycrystalline samples with the possible spatial resolution currently on the scale of a few tens of nanometers.

The geometry of the Kikuchi bands in the backscatter diffraction patterns was related to the crystal structure right from the beginning. However, it has only recently become feasible to reproduce the details and relative intensity distributions of backscatter diffraction patterns in computer calculations using the dynamical theory of electron diffraction [4,5]. The availability of these calculations makes a more rigorous comparison with experiments highly desirable.

Detecting backscatter diffraction patterns directly by a phosphor screen (or on photographic film) has the big advantage of simultaneously displaying the pattern over a very large solid angle at high angular resolution, but it is hard to get fully quantitative intensities from these measurements. There is only limited information about the energy of the electrons that hit the phosphor screen (they only have to be energetic enough to cause the emission of light) and hence it is impossible to research the significant role of inelastic energy losses in these patterns. Energy filtering of backscatter patterns has been shown to improve their contrast and sharpness [6], using a high-pass grid-based filtering setup with reported $<10$ eV energy resolution. More detailed investigations of the correlation between inelastic scattering, diffraction contrast and depth sensitivity at higher energy resolution are clearly needed and can be expected to increase the value of the EBSD method for nanoscale crystallography.

At lower energies of up to a few keV, backscattered intensity distributions have also been measured using electrostatic analyzers, in setups very similar to those used for element specific X-ray photoelectron diffraction [7]. The best of these analyzers nowadays can provide a resolution in the meV range for high resolution electron spectroscopy in the kinetic energy range up to about 1.5 keV. If the angular resolution of the measurements is good enough, clear Kikuchi features can also be observed in this energy range [8–10]. At lower angular resolution, the Kikuchi

* Corresponding author. Tel.: +61 2 61254985.
*E-mail address:* maarten.vos@anu.edu.au (M. Vos).

0304-3991/$ - see front matter © 2009 Elsevier B.V. All rights reserved.
doi:10.1016/j.ultramic.2009.05.004

features are hard to detect, but the strong forward scattering effects remain and enhance the intensity along major crystallographic directions. This can be used to determine the short-range order around the respective emitters. Due to the increased inelastic mean free paths and correspondingly larger crystal volumes probed at higher energies, the Kikuchi bands become sharper and show intricate details which are characteristic of the long-range crystal order. However, investigations using electrostatic analyzers at higher kinetic energies are affected by fundamental design limitations involving the simultaneous requirements of operation at voltages of a few tens of keV, sufficient energy resolution, and a large enough angular acceptance angle at adequate angular resolution to be able to detect diffraction features over several degrees total extension with high-resolution fine structure.

This paper is a first investigation of details of Kikuchi band formation in the energy range between 25 and 40 keV using a special electrostatic analyzer providing sub-eV energy resolution at these high energies. We analyze diffraction profiles of the quasi-elastically backscattered electrons, as well as of electrons that have experienced a well-defined number of plasmon losses. The experimentally measured diffraction profiles are compared with theoretical simulations.

## 2. Experimental details

The spectrometer used was developed for electron momentum spectroscopy and can measure electrons in an energy range from 5 to 40 keV. For a full description of the spectrometer see Ref. [11]. The geometry is sketched in Fig. 1. In brief, a well-collimated beam (divergence of the order of 0.1°, diameter 0.25 mm, directed in the horizontal plane in a direction taken as the $z$-axis) with an energy between 25 or 40 keV hits the target. A conical slit (0.2 mm wide, placed 13 cm away from the sample) selects electrons that are scattered through an azimuthal angle $\theta_{scat} = 44.3^\circ$ over a polar angle range $\phi$ from $-5$ to $5^\circ$ (these electrons travel close to the horizontal plane as well). The selected electrons enter a conical slit lens, are decelerated, and detected by a hemispherical analyzer operating at a pass energy of 200 eV. The analyzer is equipped with a pair of channel plates in a Chevron configuration followed by a resistive anode, allowing simultaneous detection of electrons over a 20 eV wide range as well as resolving the $\phi$ coordinate of the detected electron. The angular range is calibrated by replacing the entrance slit by a set of apertures, positioned at known distances along the same cone. The angular resolution obtained in this way is $\approx 0.1^\circ$. The energy resolution of the spectrometer is 0.5 eV. Energy loss spectra extending up to 60 eV were measured.

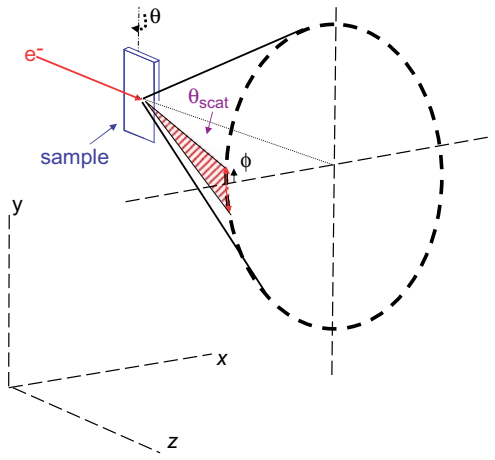


**Fig. 1.** A sketch of the experimental geometry. The incoming electrons impinge at the sample at a glancing angle ($\approx 20^\circ$). Electrons emerging along the hatched area of a cone, with the cone axis along the incoming beam direction (cone half angle corresponds to $\theta_{scat}$ and is 44.3°) are detected. The outgoing angle of the electrons with the surface ($\theta$) can be changed by rotating the sample about the vertical axis.

Si samples ([1 0 0] surface normal) were sputter cleaned by bombarding the sample with 1.2 keV Xe ions. The sample was subsequently annealed at temperatures high enough for the implanted Xe to desorb. From infra-red pyrometer readings we conclude that this happens at, or above, the temperature for which epitaxial regrowth occurs of the amorphized layer, produced by Xe sputtering. The samples were subsequently transferred under UHV to the main spectrometer with an operating pressure of $1 \times 10^{-10}$ torr. No deterioration of the spectrum could be noticed over the measurement period (several days). The sample can be rotated about the vertical axis such that the incoming and outgoing angles change. The accuracy of the rotation was about 0.2°. However, the absolute angle (e.g. the angle that would correspond to the incoming beam impinging along the surface normal) is known with an accuracy of only1°–2°.

## 3. Theory

The theory used is described in detail elsewhere [4]. Our calculations are closely related to the theory of electron channeling patterns [12] ruled by diffraction of the incoming beam rather than diffraction of the outgoing beam as is the case in backscatter diffraction. The two approaches are related by the reciprocity principle, which allows us (for the case of quasi-elastic scattering) to calculate the diffracted backscattered intensities as a time-reversed channeling pattern of electron plane waves that travel backwards from the directions measured by the electron energy analyzer to the sample.

In brief, the wave function inside the crystal is described as a superposition of Bloch waves with wave vectors $\mathbf{k}^{(j)}$

$$\Psi(\mathbf{r}) = \sum_j c_j \exp(i\mathbf{k}^{(j)} \cdot \mathbf{r}) \sum_g C_g^{(j)} \exp(i\mathbf{g} \cdot \mathbf{r}) \quad (1)$$

and we then solve for the expansion coefficients $c_j$ and $C_g^{(j)}$, as well as the $\mathbf{k}^{(j)}$ by inserting (1) into the Schrödinger equation. The scattering potential is assumed to have the bulk symmetry. By introducing the high-energy forward-scattering approximation, the Schrödinger equation can be transformed into an eigenvalue problem for a general complex matrix, which is solved by standard numerical procedures. The matrix dimensions are determined by the number of Fourier coefficients used to approximate the scattering potential. These coefficients are related to the respective reciprocal space vectors or reflecting sets of lattice planes $\mathbf{g}_{hkl}$.

Since we measure the quasi-elastically backscattered electrons, we know that this group of electrons is produced predominantly at the positions of the crystal atoms. We thus have to calculate the respective overlaps of the diffracted wave function with point sources centered at the positions of the Si atoms, broadened by thermal vibrations.

The following parameters were used in the theoretical calculations shown below. The lattice constant of Si was taken as $a_{Si} = 0.5431$ nm. From a total set of about 3100 reciprocal space vectors $\mathbf{g}_{hkl}$ with minimum lattice spacing $d_{hkl} = 0.045$ nm, an average number of about 170 strong reflections was selected for exact diagonalization, the rest was included by Bethe perturbation. An inelastic mean free path (in nm) of $\lambda_i = 0.0116E^{0.775}$ (with $E$ in eV), in silicon was assumed [13], resulting in $\lambda_i = 43$ nm at

$E = 40$ keV and $\lambda_i = 30$ nm at $E = 25$ keV. Thermal vibrations are included via a Debye–Waller factor of 0.005 nm$^2$.

We assume here that the possible channeling of the incident beam does not affect the angular distribution in the exit path. The backscattered electrons are taken to be completely incoherent with respect to the incident beam since no diffraction spots are observed.

## 4. Results

An example of a spectrum obtained for 40 keV electrons (wavelength $\lambda = 0.0060$ nm) scattered from Si, integrated over all $\phi$ angles is shown in Fig. 2. The (quasi-)elastic peak is taken at zero energy loss and is followed by a broader structure due to electrons that have created electronic excitations in Si. The width of the elastic peak is in part due to energy resolution of the spectrometer, and in part due to Doppler broadening of the peak due to vibrations of the Si nuclei (see e.g. [14]) (experimental resolution of the spectrometer $\approx 0.6$ eV, Si peak width $\approx 1.2$ eV at 40 keV, hence Doppler broadening $\approx 1.0$ eV). Besides the effect of surface excitations (around $\simeq 12$ eV) we see peaks due to electrons that have excited 1 (at $\simeq 17$ eV energy loss), 2 (at $\simeq 34$ eV) and 3 (at $\simeq 51$ eV) plasmons.

In these measurement we change gradually the float voltage of the analyzer. In this way we obtain the spectrum over a larger range than the energy window of the analyzer itself. Another important consequence is that scanning of the float voltage removes the effect on the spectrum of the varying efficiency of the multi-channel plates, as each position of the channel plate contribute (depending on the analyzer float voltage) to all energy loss channels.

If we integrate the spectrum from the elastic peak up to 55 eV energy loss, and plot the intensity as a function of angle then we obtain an angular distribution with varying intensity. However, a certain position of the two-dimensional detector corresponds always to the same $\phi$ angle. Thus at least part of the intensity variation obtained in this way is due to the varying efficiency of the channel plates. This can be divided out by measuring the angular yield of electrons backscattered from a stainless steel shim as explained in Fig. 3. After division, the distribution obtained is symmetric around $\phi = -0.45°$. The Si(1 0 0) crystal was inserted in the sample holder with the [0 1 1] direction approximately vertical (easily identified by the cleavage planes of Si). Thus we assume that the symmetry in the angular distribution corresponds to the (0 1 1) symmetry plane being directed towards the analyzer. A 0.45° offset is reasonable considering the accuracy of the alignment procedure used. From here on we have always adjusted the $\phi$ scale in such a way that $\phi = 0$ corresponds to the symmetry point.

The normalized distribution has a band of increased intensity for $|\phi| < 1.4°$. We identify this as the Kikuchi band associated with

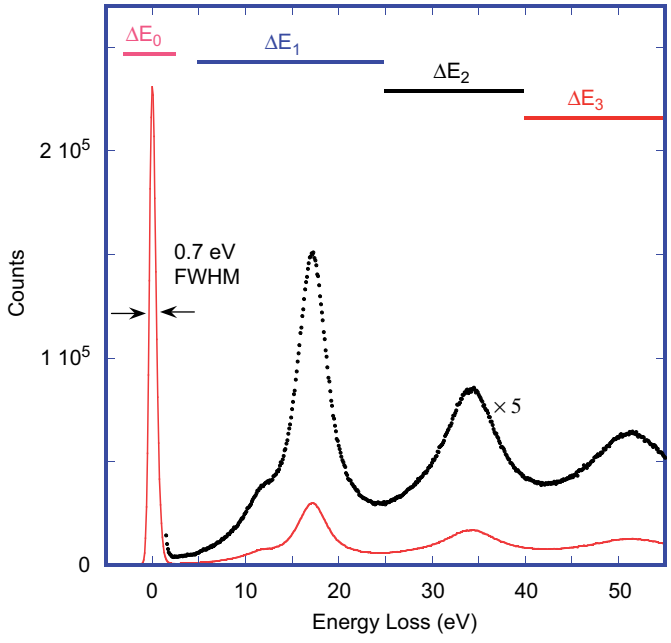


**Fig. 2.** A spectrum from Si, obtained at 40 keV, integrated over all detected angles $\phi$.

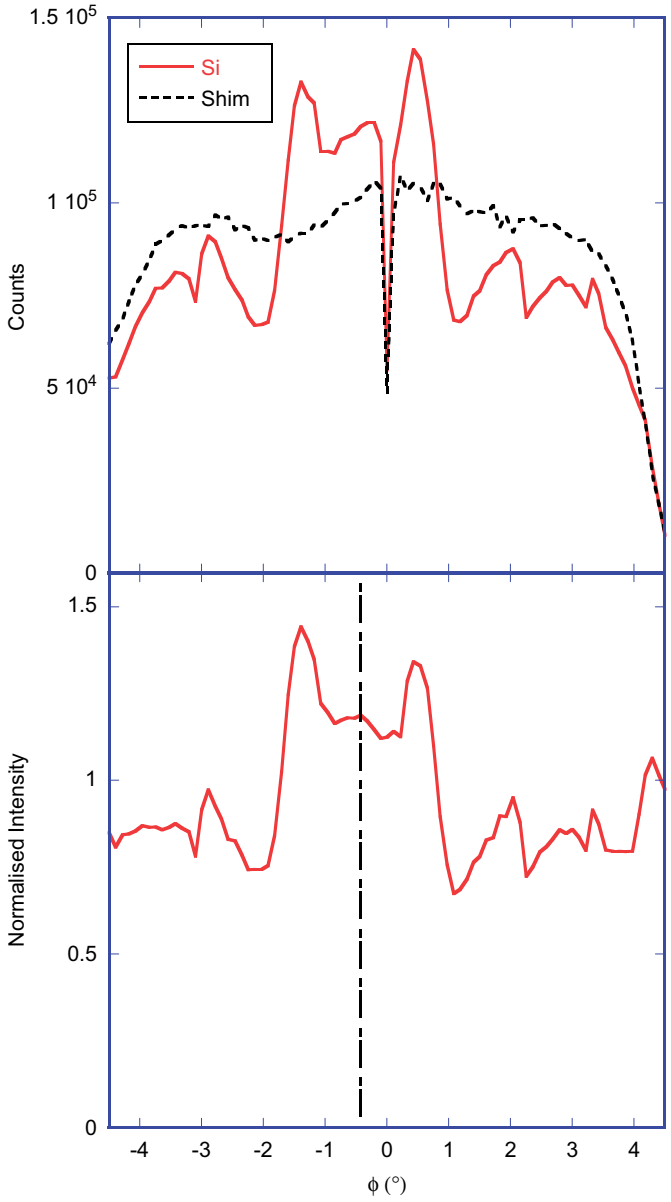


**Fig. 3.** The angular yield from a Si single crystal and a polycrystalline metal shim. The sharp dip in the middle is due to thin metal hairline over the entrance slit used for the sample alignment. The rest of the structure in the angular distribution of electrons scattered from the shim is due to varying channel plate efficiency. Near the edges, the gradual decline of the distribution is due to the fact that large angles are measured less efficiently in our spectrometer, using round channel plates. The division of the Si distribution by the shim distribution (bottom panel) leaves us with intensity variations due to crystalline effects. This pattern is symmetric around $\phi = -0.45°$.

the (0 2 2) plane. The width of a Kikuchi band is (as a rough estimate) usually taken to be twice the Bragg angle: $\simeq \lambda/D$. For the (0 2 2) plane of Si (lattice plane $d$-spacing $D = 0.192$ nm) this correspond to 1.8°. The observed width ($2 \times 1.4 \sin 44.3^\circ = 1.95^\circ$) is indeed close to this estimate. However, on top of the main band there appear additional fine structures. This fine structure

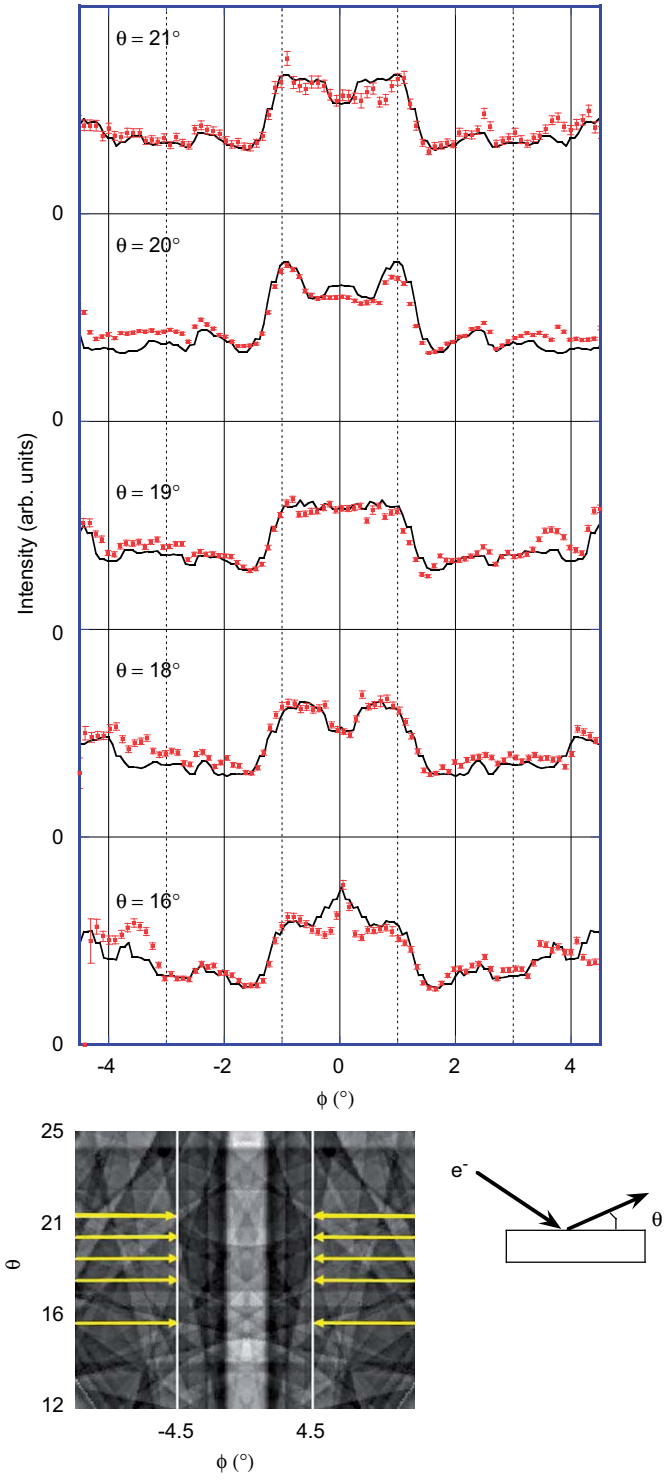


**Fig. 4.** The top panel shows the spectra measured for the rotational angles as indicated (data points), compared to the calculated results (solid line). The theoretical calculations are also shown as a gray-scale image in the bottom left panel. The measurements extend, along a slightly curved line, between the arrows. A top view of the measurement geometry, and the definition of $\theta$ is shown in the lower-right part of the figure.

changes if we rotate the sample around the vertical axis (i.e. the (0 2 2) plane remains pointing towards the analyzer). This is demonstrated in Fig. 4 where we show the experimental result, after normalization by the detector response function. Indeed there is always a clear band of increased intensity visible, of roughly constant width. A detailed look at the line shapes reveals clear changes, e.g. sometimes a maximum appears at $\phi = 0^\circ$, sometimes there is a local minimum at this angle. The calculated Kikuchi pattern is also shown in Fig. 4 as a gray-scale image. For comparison of experiment and theory we have to know the relation between the sample rotation, as measured from the vacuum motion feed-through, and the actual angle between the outgoing electron trajectories and the sample surface. The top spectrum of the figure shows a maximum at $\phi = 0^\circ$. At the nominal $\theta$ angle of 17.5° there is no such maximum. In the theory the closest maximum at $\phi = 0$ occurs at $\theta \simeq 16^\circ$. Such a deviation is compatible with the experimental uncertainty. Hence we conclude that this spectrum was taken in fact at 16°. After establishing this, we know the $\theta$ angle of the other measurements with a much higher accuracy (±0.2°). Hence we compare all these measurements with the theory using this angular calibration in Fig. 4. The agreement, especially of the shape of the main Kikuchi band is very good. The vertical scale for the theory was adjusted for a best agreement with experiment. There is no offset in the comparison of theory and experiment, i.e. zero intensity of the experiment corresponds to the zero intensity of the theory. Thus the magnitude of the intensity modulation predicted by theory is reproduced by the experiment.

In a different experiment we investigated the dependence of the observed pattern on the energy of the incoming electrons. This measurement was nominally done at the same orientation as the 20° measurement of Fig. 4, but we obtained slightly better agreement with experiment if we compared this measurement with calculations at 20.15°. This is done in Fig. 5. There is in the experiment, a slow but noticeable increase in the total width of the main Kikuchi band. The changes in the detail of the shape are much more dramatic, and are faithfully reproduced by the theory. The broad valley, visible in the middle of the band (with possible a slight maximum at $\phi = 0^\circ$) narrows with decreasing energy, and a sharp peak appears at $\phi = 0^\circ$ at 25 keV. Even the minor features, at larger $\phi$ angles are generally seen in both theory and experiment.

Thus far we obtained the angular spectrum by integrating over energy from the elastic peak to 55 eV energy loss. This maximizes the statistics in the angular distribution pattern. We can, especially for those measurements where many counts were acquired, plot the angular distribution for selected energy loss regions. This is done in Fig. 6 for the energy regions shown in Fig. 2. All angular distributions were normalized such that the maximum intensity was 1. The same structures are seen for all distributions, however, the amplitude of the intensity variations decreases slowly, but noticeably with increasing energy loss.

In Figs. 2–4 we showed the intensity integrated up to 55 eV, which improves the signal-to-noise ratio. This distribution is shown as well in Fig. 6. It shows indeed slightly less structure than the distribution obtained from the elastic peak only. Similar conclusions were reached for electron channeling measurements in an electron microscope [15].

The large-angle quasi-elastic scattering effect is localized at an atomic position. The outgoing waves, originating from this position, interfere with the crystal (a "three-dimensional diffraction grating") to produce the Kikuchi pattern. Inelastic events along the outgoing trajectory will affect the phase of the outgoing electron, and hence it loses its capability to form an interference pattern depending on the properties of the inelastic scattering effects. In the calculation these effects are included via an

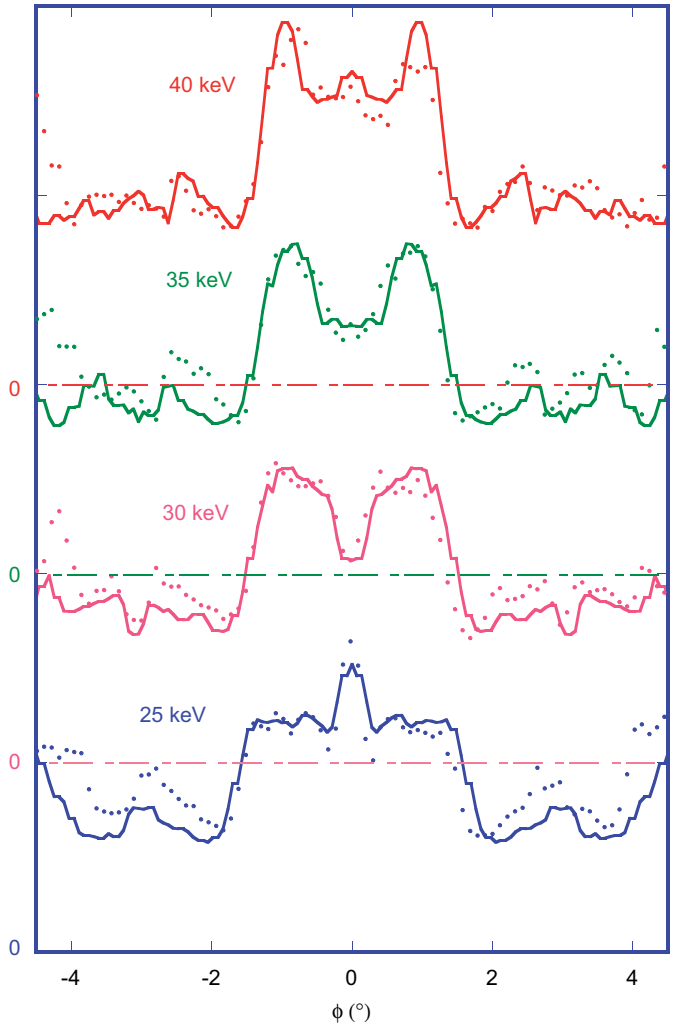


**Fig. 5.** The effect of $E_0$ on the measured angular intensity distribution.

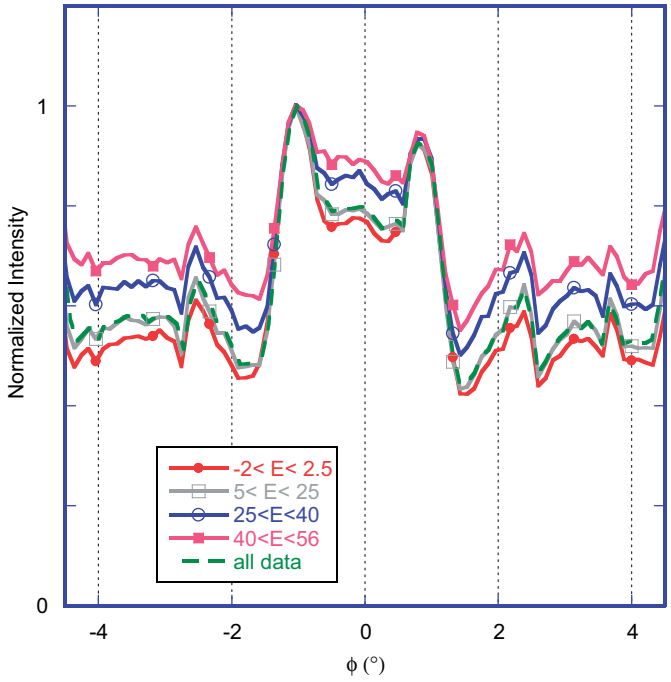


**Fig. 6.** Angular distribution obtained from the spectra integrated over the energy loss regions (in units of eV), as indicated. The corresponding regions are indicated in Fig. 2 as well, and correspond roughly to 0–3 inelastic excitations created by the electrons in the crystal. With increasing energy loss, the contrast of the angular distribution is decreased. The angular distribution of all data is shown as a thin solid line.

imaginary part of the potential. This potential simply accounts for the loss of electrons from the outgoing channel, aloss that increases with the path length traveled in the crystal. In reality these electrons do not really disappear, but will hit the phosphor screen at slightly lower energy. Thus the calculation applies in this respect to the angular pattern of the elastic peak, not the image seen on a phosphor screen.

It is interesting to look at the decline in contrast with increasing energy loss. If we assume that electrons in the $\Delta E_3$ window (see Fig. 2) have created on average three plasmons, then one can calculate, assuming equal path length of the incoming and outgoing trajectories, that only in $(1/2)^3 = 1/8$ of all cases is there no plasmon created for the outgoing trajectory. The decrease in contrast is less dramatic, so it is directly seen that electrons which have excited a small number of plasmons can still show a significant diffraction contrast. This is related to the delocalized nature of the plasmons [16] and it is well known in energy-filtered transmission electron microscopy that diffraction contrast is partially preserved after plasmon losses [17].

However, these results are in clear contrast with the conclusion reached by Deal et al. [6], that maximum contrast is reached for electrons with energy several hundred eV less than the primary energy. A possible explanation of the results of Deal et al. would be that trajectories of electrons passing through their high-pass grid with energies close to the cut-off value are affected by the grid and hence do not form a contrast-rich image.

Future investigations are planned to measure the contrast development over a larger window of electron energy losses, thus giving insight into the correlation between inelastic scattering and the amount of remaining crystallographic information that was initially provided by the localized nature of the quasi-elastic backscattering process.

## 5. Conclusions and outlook

It is demonstrated that it is possible to quantitatively measure details of angular profiles in Kikuchi patterns of backscattered electrons in the energy range of 25–40 keV using an electrostatic analyzer. The agreement with recent theories is good. These experiments make it possible to study the effect of additional inelastic scattering events on the angular distribution of the emerging electrons.

Channeling effects in the incident beam, which have been neglected in this study, can be expected to influence the backscattered electron profiles. Although, in the general case, the simulation of such double-channeling effects is significantly more complicated [18], considerable simplifications should be possible when ingoing and outgoing channeling can be assumed to be largely incoherent with respect to each other. Then the ingoing channeling, in a first approximation, should mainly scale the overall intensity of diffraction profiles that have been obtained for different incidence angles. The respective scale factors could then be obtained from a channeling calculation for the corresponding incidence geometry.

In the present experiment we used a rather small scattering angle (44.3°). By increasing the scattering angle we can access a larger range of incoming and outgoing trajectories. This will make it possible to align the major crystallographic directions with the analyzer, the case where the enhancement of the intensity is largest. Increasing the scattering angle also makes the energy

transfer in the (quasi-)elastic scattering event larger (recoil effect) and it becomes possible to separate the quasi-elastic peak in different components due to atoms of different mass [19]. Thus by studying, for example, a Si crystal with an epitaxial Ge layer, then the angular distribution of the Ge elastic peak is due to scattering from a surface layer of well-defined thickness. Such experiments can further test our understanding of the interaction of keV electrons with matter, and open up a novel way of studying nanostructured layers.

## Acknowledgments

This research was made possible by a grant of the Australian Research Council. We thank Les Allen for stimulating discussions and Erich Weigold for critically reading the manuscript.

## References

[1] S. Kikuchi, Diffraction of cathode rays by mica, Proc. Imp. Acad. 4 (1928) 354–356.
[2] S. Nishikawa, S. Kikuchi, The diffraction of cathode rays by calcite, Proc. Imp. Acad. 4 (1928) 475–477.
[3] A. Wilkinson, P.B. Hirsch, Electron diffraction based techniques in scanning electron microscopy of bulk materials, Micron 28 (1997) 279–308.
[4] A. Winkelmann, C. Trager-Cowan, F. Sweeney, A.P. Day, P. Parbrook, Many-beam dynamical simulation of electron backscatter diffraction patterns, Ultramicroscopy 107 (2007) 414–421.
[5] A. Winkelmann, Dynamical effects of anisotropic inelastic scattering in electron backscatter diffraction, Ultramicroscopy 108 (2008) 1546–1550.
[6] A. Deal, T. Hooghan, A. Eades, Energy-filtered electron backscatter diffraction, Ultramicroscopy 108 (2008) 116–125.
[7] S. Chambers, Elastic scattering and interference of backscattered primary, Auger and X-ray photoelectrons at high kinetic energy: principles and applications, Surf. Sci. Rep. 16 (1992) 261–331.
[8] J. Osterwalder, R. Fasel, A. Stuck, P. Aebi, L. Schlapbach, Holographic interpretation of photoelectron diffraction, J. Electron Spectrosc. Relat. Phenom. 68 (1994) 1–18.
[9] T. Katayama, H. Yamamoto, Y.M. Koyama, S. Kawazu, M. Umeno, Kikuchi-band analysis of X-ray photoelectron diffraction fine structure of Si(1 0 0) by precise angle-resolved X-ray photoelectron spectroscopy, Jpn. J. Appl. Phys. 38 (1999) 1547–1552.
[10] L. Broekman, A. Tadich, E. Huwald, J. Riley, R. Leckey, T. Seyller, K. Emtsev, L. Ley, First results from a second generation toroidal electron spectrometer, J. Electron Spectrosc. Relat. Phenom. 144–147 (2005) 1001–1004.
[11] M. Vos, G.P. Cornish, E. Weigold, A high-energy (e,2e) spectrometer for the study of the spectral momentum density of materials, Rev. Sci. Instrum. 71 (2000) 3831–3840.
[12] C.J. Rossouw, P.R. Miller, T.W. Josefsson, L.J. Allen, Zone-axis back-scattered electron contrast for fast electrons, Philos. Mag. A 70 (1994) 985–998.
[13] S. Tanuma, C.J. Powel, D.R. Penn, Calculation of electron inelastic mean free paths, Surf. Interface Anal. 20 (1993) 77–89.
[14] M. Vos, M.R. Went, Effects of bonding on the energy distribution of electrons scattered elastically at high momentum transfer, Phys. Rev. B 74 (2006) 205407.
[15] D.C. Joy, D. Newbury, D. Davidson, Electron channeling patterns in the scanning electron microscope, J. Appl. Phys. 53 (1982) R81–R122.
[16] A. Howie, Inelastic scattering of electrons by crystals I. The theory of small-angle inelastic scattering, Proc. R. Soc. London A 271 (1963) 268–287.
[17] H. Watanabe, Energy selecting microscope, Jpn. J. Appl. Phys. 3 (1964) 480–485.
[18] L.J. Allen, S.D. Findlay, M.P. Oxley, C. Witte, N.J. Zaluzec, Channeling effects in high-angular-resolution electron spectroscopy, Phys. Rev. B 73 (2006) 094104.
[19] M. Vos, M. Went, Rutherford backscattering using electrons as projectiles: underlying principles and possible applications, Nucl. Instrum. Methods B 266 (2008) 998–1011.